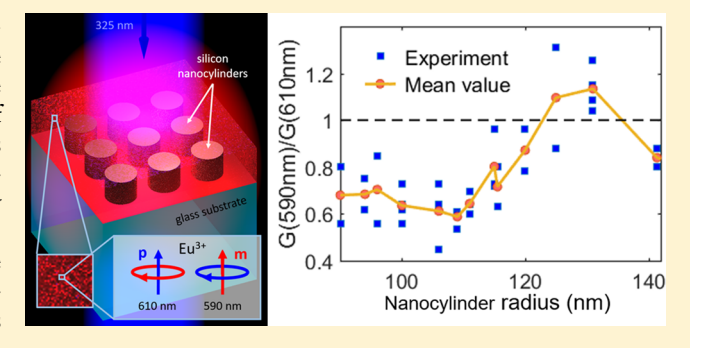
Manipulation of Magnetic Dipole Emission from Eu³⁺ with Mie-**Resonant Dielectric Metasurfaces**

Aleksandr Vaskin,*,†© Soheila Mashhadi,[‡] Michael Steinert,[†] Katie E. Chong,[§] David Keene,[‡] Stefan Nanz,^{||} Aimi Abass,[†] Evgenia Rusak,^{||,§} Duk-Yong Choi,[‡] Ivan Fernandez-Corbaton,[†]© Thomas Pertsch,[†] Carsten Rockstuhl,^{†,||} Mikhail A. Noginov,[‡] Yuri S. Kivshar,[§]© Dragomir N. Neshev, Natalia Noginova, and Isabelle Staude

Supporting Information

Downloaded by NORFOLK STATE UNIV at 14:17:29:660 on July 02, 2019 from https://pubs.acs.org/doi/10.1021/acs.nanolett.8b04268.

ABSTRACT: Mie-resonant high-index dielectric nanoparticles and metasurfaces have been suggested as a viable platform for enhancing both electric and magnetic dipole transitions of fluorescent emitters. While the enhancement of the electric dipole transitions by such dielectric nanoparticles has been demonstrated experimentally, the case of magneticdipole transitions remains largely unexplored. Here, we study the enhancement of spontaneous emission of Eu3+ ions, featuring both electric and magnetic-dominated dipole transitions, by dielectric metasurfaces composed of Mieresonant silicon nanocylinders. By coating the metasurfaces with a layer of an Eu³⁺ doped polymer, we observe an



enhancement of the Eu³⁺ emission associated with the electric (at 610 nm) and magnetic-dominated (at 590 nm) dipole transitions. The enhancement factor depends systematically on the spectral proximity of the atomic transitions to the Mie resonances as well as their multipolar order, both controlled by the nanocylinder size. Importantly, the branching ratio of emission via the electric or magnetic transition channel can be modified by carefully designing the metasurface, where the magnetic dipole transition is enhanced more than the electric transition for cylinders with radii of about 130 nm. We confirm our observations by numerical simulations based on the reciprocity principle. Our results open new opportunities for bright nanoscale light sources based on magnetic transitions.

KEYWORDS: Magnetic dipole emission, dielectric metasurfaces, Mie resonances, Purcell enhancement

n optics, the interaction of matter with the magnetic field of light is usually ignored since it is several orders of magnitude weaker as compared to the interaction of matter with the electric field of light. 1-3 An important exception, however, is exemplified by trivalent lanthanide ions, such as Eu3+ and Er3+, which are well-known to exhibit magneticdipole transitions in the visible and near-infrared region, respectively. Trivalent lanthanides have been intensely studied for a few decades and remain an active subject of research.^{3–5} Recently, for example, Kasperczyk et al.4 demonstrated that the magnetic dipole transition of Eu³⁺ ions can be selectively excited using azimuthally polarized focused laser beams possessing high magnetic and vanishing electric field at the

center. As such, the engineering of the optical excitation has proven to be an effective way to influence how lanthanide ions interact with light.

Another important factor governing the light-matter interaction of lanthanide ions is their photonic environment. It has a crucial influence on the spontaneous emission via both electric and magnetic dipole transitions. This influence was first described by Purcell for magnetic dipole radiation and later generalized for both electric and magnetic emission

Received: October 23, 2018 Revised: December 29, 2018 Published: January 3, 2019



[†]Institute of Applied Physics, Abbe Center of Photonics, Friedrich Schiller University Jena, 07745 Jena, Germany

^{*}Center for Materials Research, Norfolk State University, Norfolk, Virginia 23504, United States

[§]Nonlinear Physics Centre, Research School of Physics and Engineering, The Australian National University, Canberra, ACT 2601, Australia

Institute of Theoretical Solid State Physics, Karlsruhe Institute of Technology, 76131 Karlsruhe, Germany

¹Institute of Nanotechnology, Karlsruhe Institute of Technology, 76021 Karlsruhe, Germany

Laser Physics Centre, Research School of Physics and Engineering, The Australian National University, Canberra, ACT 2601,

through the so-called Purcell factor (see Baranov et al. of a recent review). Thus, proper engineering of the photonic environment could dramatically influence the selectivity between the electric and magnetic emission channels. In that respect, optical metamaterials and metasurfaces offer unique opportunities for designing the electric and magnetic near-field environment and hence for selectively enhancing the emission rates of electric or magnetic emitters.

Indeed, the modification of the local density of optical states (LDOS) and the manipulation of magnetic dipole spontaneous emission have been studied using various photonic structures, setuctures, and plasmonic micro- and nanostructures. Resonant plasmonic metasurfaces consisting of an array of nanoholes in a bilayer gold film have shown a clear difference in the enhancement of the magnetic dipole transition with respect to the electric transition. Designed to support plasmonic resonances overlapping with the emission spectrum of the Eu³⁺ ions, the nanohole metasurface allowed for preferential enhancement only of the magnetic emission.

However, in the vicinity to plasmonic nanostructures the intrinsic absorption losses of metals at optical frequencies can result in quenching of the emission. To overcome this limitation, high-index dielectric nanoparticles and metasurfaces $^{16-21}$ have been suggested as an alternative platform to efficiently tailor the magnetic LDOS and selectively enhance magnetic radiative decay. For a sufficiently high index contrast to the environment, dielectric nanoparticles can support both electric and magnetic multipolar Mie-type resonances in the visible, which can be tailored by the nanoparticle geometry. In particular, it was shown theoretically that near-infrared quadrupolar magnetic resonances in silicon particles can preferentially promote magnetic versus electric radiative de-excitation in trivalent erbium ions at $1.54~\mu \mathrm{m}.^{22}$

The enhancement of the magnetic dipole emission was also studied, both analytically and numerically, for a variety of dielectric nanoparticles, including nanospheres²⁴ and hollow nanodisks. 25,26 In the latter case, it was predicted that the emission can be significantly enhanced near the magnetic dipole resonance, while electric dipole emission will be suppressed when emitters are located in a hollow of the nanodisk.²⁵ In a recent experimental work, Sanz-Paz et al. mapped the spatial distributions of the relative magnetic and electric radiative LDOS and showed magnetic emission enhancement near single photonic nanoantennas, which were carved by a focused-ion beam (FIB) at the extremity of a nearfield tip.²⁷ Specifically, two nanoantennas with fixed geometrical parameters, namely one magnetic dipolar silicon antenna and one electric monopolar aluminum antenna, were realized and scanned over Eu³⁺-doped nanoparticles to record the spatial distributions of the electric and magnetic density of states. However, the overall magnetic emission enhancement mediated by a single silicon nanoantenna exhibiting a magnetic dipole resonance was rather small. Sanz-Paz et al. estimate a 2× average enhancement in their system. The scanning probe geometry also makes it difficult to compare the emission in the presence of the nanoantenna with the reference case without any nanoantenna, as well as to vary the antenna dimensions to investigate the influence of the resonance position on the enhancement. Wiecha et al.²⁸ also investigated the interaction of individual dielectric nanostructures with electric and magnetic dipole transitions, in their case supported by a few

nanometer thin film of rare-earth ion doped clusters. They recorded the photoluminescence from the layer excited by a focused laser beam to simultaneously map the electric and magnetic emission enhancement on single silicon nanorods and dimers. An enhancement of the luminescence intensity by a factor of around 3 for the magnetic dipole transition and by 1.5 for the electric dipole transition was found.

In order to increase the average magnetic enhancement values, nanophotonic architectures supporting Mie-type resonances of quadrupolar or higher order are promising. In this work, we probe experimentally, for the first time to the best of our knowledge, the modification of spontaneous emission via electric and magnetic channels by dielectric metasurfaces consisting of silicon nanocylinders supporting quadrupolar-dominated resonances. Moreover, using metasurfaces for this purpose is interesting by itself, as they offer many degrees of freedom for tailoring and enhancing spontaneous emission, including the nanoresonator arrangement and geometry as well as in-plane spatial variations of thereof. ^{29–31} The metasurfaces are covered by a thin layer of a Eu³⁺ containing polymer, as conceptually illustrated in Figure 1. We fabricate different metasurfaces featuring a systematic

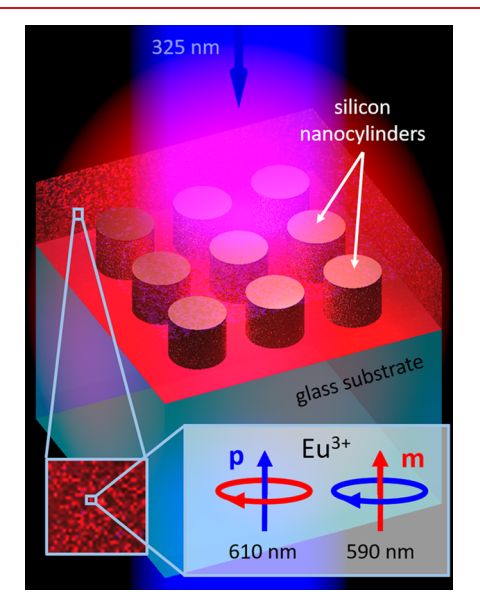


Figure 1. Artist's impression of Mie-resonant silicon nanocylinders covered by a thin layer of Eu^{3+} containing polymer.

variation of the nanocylinder radius, which allows us to sweep the spectral position of the quadrupolar-dominated resonances over the emission band of the Eu3+. We map selectively the emission of the Eu3+ ions at the electric and magnetic transition at 610 and 590 nm, respectively, as a function of the nanocylinder radius, reaching a maximum absolute averaged magnetic (electric) emission enhancement by a factor of 6.5 (8). Importantly, the maximum enhancements for the two channels are realized for different nanocylinder radii, showing that Mie-resonant all-dielectric metasurfaces allow for selective enhancement of the magnetic dipole over the electric dipole emission, for a proper choice of the metasurface geometry. For further quantitative analysis, we also determine the ratio of the emission enhancements via the two distinct channels. We support our experimental observations with numerical simulations taking the periodic boundary conditions of the

metasurface and the random position and orientation of the emitters in the film into account.

Results and Discussion. We fabricated two identical samples, each consisting of 20 nanocylinder metasurfaces with a footprint of $100~\mu m \times 100~\mu m$ and nanocylinder radii varying between 96 and 146 nm (see Methods for details on the fabrication process). The lattice constant and cylinder height were fixed to 560 and 182 nm, respectively. Two identical samples were fabricated to allow for assessing the variability of the results. For the same reason, each sample features additional redundancies in the nanocylinder sizes. A scanning-electron microscope (SEM) image of one of the fabricated metasurfaces is shown in Figure 2a.

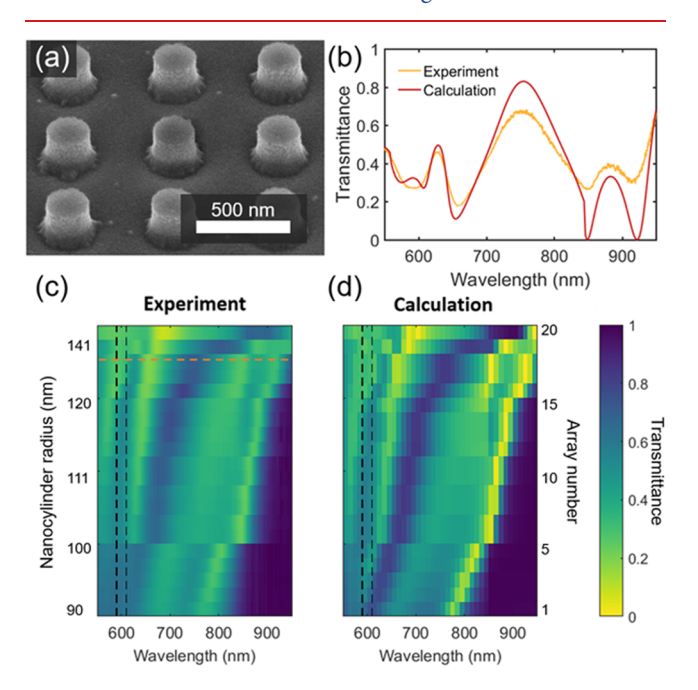


Figure 2. (a) Scanning electron micrograph of a typical silicon metasurface array before coating with the Eu³⁺ containing layer. (b) Experimentally measured and numerically calculated transmittance of a silicon metasurface with a nanocylinder radius of 131 nm. (c,d) Experimental and numerically calculated transmittance spectra for a series of silicon metasurfaces featuring a variation of the nanocylinder size, displayed in dependence of the nanocylinder radius and the corresponding array number. Note that the increase in nanocylinder size with growing array number happens in nonequidistant steps. For a table summarizing the exact geometrical parameters (radius, height) of all studied samples, please refer to the Supporting Information. The dashed vertical lines indicate the wavelengths of the MD transition at 590 nm and ED transition at 610 nm of Eu³⁺. The dashed horizontal line corresponds to the sample depicted in (b).

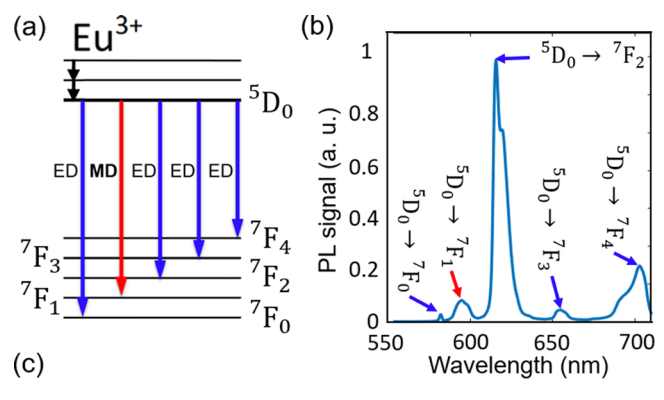
As the first step, the fabricated metasurfaces were characterized using near-normal incidence linear-optical transmittance spectroscopy. A typical experimental transmittance spectrum is shown in Figure 2b (yellow line). The spectrum exhibits several pronounced minima corresponding to Mietype resonances of the silicon nanocylinders. Figure 2b also shows a corresponding numerically calculated transmittance spectrum obtained via finite-element calculations using the software package COMSOL Multiphysics (see Methods for details). In order to match the spectral position of the minima with those observed in the experiments, the height and radius of the cylinders were varied within the experimental accuracy

limits, while the period was kept constant at its design value. Furthermore, we performed a multipole decomposition³² of the modes excited in the silicon nanocylinders (see Figure.S2 of the Supporting Information for the multipole decomposition results), revealing that the minimum at 920 nm in Figure 2b corresponds to the excitation of a magnetic dipole (MD) resonance, the minimum at 850 nm corresponds to an electric dipole (ED) resonance, and the minima at wavelengths below 700 nm originate from the excitation of the electric and magnetic quadrupole-dominated modes. We measured the transmittance spectra for all 20 metasurfaces, each having different nanocylinder radius. As can be seen in Figure 2c, in the transmittance spectra, the Mie-resonances are red-shifting with increasing nanocylinder radius. The metasurfaces are sorted such that a larger array number corresponds to a larger radius. Corresponding calculated transmittance spectra are depicted in Figure 2d. From our calculations, we can identify the effective nanocylinder height and radius for each of the metasurfaces by optimizing the agreement of the calculated transmittance spectrum with the respective experimental spectrum (see Table S1 of the Supporting Information for the obtained metasurface geometrical parameters). We were able to precisely match the experimentally observed resonance positions, however, a discrepancy in the absolute transmittance levels remains, which we attribute to sample imperfections, such as surface roughness. The difference between the nanocylinders sizes used in calculations and measured in a SEM is within a range of 20 nm. This small difference is likely due to the formation of a low-index layer at the surface of the nanocylinders, deviations of the silicon refractive index in the nanostructured sample as compared to the unstructured film used in ellipsometry measurements, and a slight tilt of the nanocylinder side walls.3

In Figure 2c,d, the wavelengths of 590 and 610 nm, which correspond to the magnetic-dominated and electric dipole transitions of $\mathrm{Eu^{3+}}$, respectively, are indicated as dashed lines. The spectral overlap of these transitions with the Mieresonances varies for different nanocylinder radii. This allows us to study the influence of the Miermodes of the nanocylinders on the enhancement of the different types of transitions in $\mathrm{Eu^{3+}}$.

As a material incorporating luminescent Eu3+, we use the alkylated europium complex (tris(α -henoyltrifluoroacetone)-(1-octadecyl-2(-2-pyridyl)benzimidazole)europium(III)) abbreviated as Eu(TTA)₃L18. The Eu(TTA)₃L18 material was prepared following the method described in Wang et al.³⁴ A schematic of the electronic energy-level structure of the Eu³⁺ in this complex is shown in Figure 3a. The material can be excited in the ultraviolet spectral range and shows emission in the visible, which is associated with several radiative decay channels having the same upper energy level 5D_0 , but several lower levels. A measured emission spectrum of Eu(TTA)₃L18 is shown in Figure 3b. The Eu³⁺ emission line at $\lambda = 590$ nm is dominated by the magnetic dipole transition ${}^5D_0 \rightarrow {}^7F_1$, while the strongest line in the emission spectrum at $\lambda = 610$ nm corresponds to the electric dipole transition ${}^5D_0 \rightarrow {}^7F_2$. Solutions of Eu(TTA)₃L18 complex and polystyrene in chloroform were mixed in the proportion 1:5 and spin coated on the metasurface array to produce a thin film with a thickness of approximately 200 nm, as measured in the unstructured areas of the sample.

A SEM image of a focused ion-beam cross section of one of the metasurfaces after application of the Eu³⁺ containing



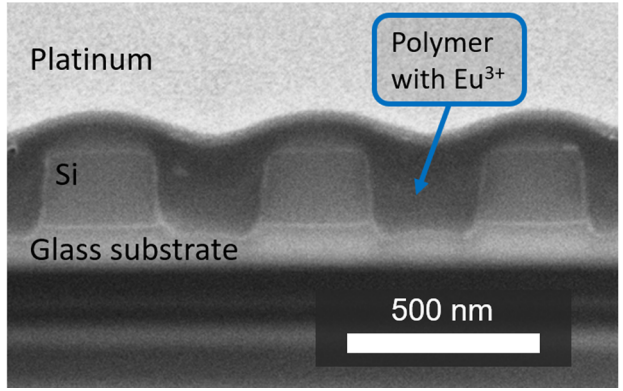


Figure 3. (a) Sketch of the energy-level structure of Eu³⁺. (b) Measured emission spectra from the Eu³⁺ containing polymer layer coated onto a bare glass substrate. (c) SEM image of a focused ion-beam cross section of one of the metasurfaces after spin coating with the Eu³⁺ containing polymer.

polymer layer is displayed in Figure 3c. Note that the application of the layer induces a slight red-shift of the resonances with respect to the spectra presented in Figure 2c, which depends on the layer thickness. Furthermore, the layer leads to a modification of the multipolar composition of the metasurface response, increasing the relative contribution of the electric quadrupole and magnetic quadrupole while decreasing the contribution of the electric dipole (see Figure.S4 of the Supporting Information).

In order to investigate the fluorescence properties of the coated metasurface arrays, the Eu³⁺ was excited with a He-Cd laser, emitting at $\lambda = 325$ nm wavelength. An 0.4NA objective was used to collect the emission from the sample. Interferometric narrow-band filters centered at 590 or 610 nm were placed in the recording channel in order to selectively detect the emission at the magnetic dipole or electric dipole transition, respectively. The emission was focused at the sensor of a Thorlabs 1500 M GE-TE CCD camera in order to record the fluorescence microscopy image. Further details on the measurement procedure including a sketch of the experimental setup are included in the Supporting Information. The results are summarized in Figure 4. Fluorescence microscope images of a set of metasurfaces covered by a Eu³⁺ containing polymer layer, taken at the magnetic and electric dipole transition wavelengths, are shown in Figure 4a,b, respectively. Both images were recorded using the same gain settings but different integration times of 4000 ms for the wavelength of 590 nm and 400 ms for the wavelength of 610 nm. This results in approximately equal intensities of the emission at 590 and 610 nm wavelength in the areas in between the metasurface arrays,

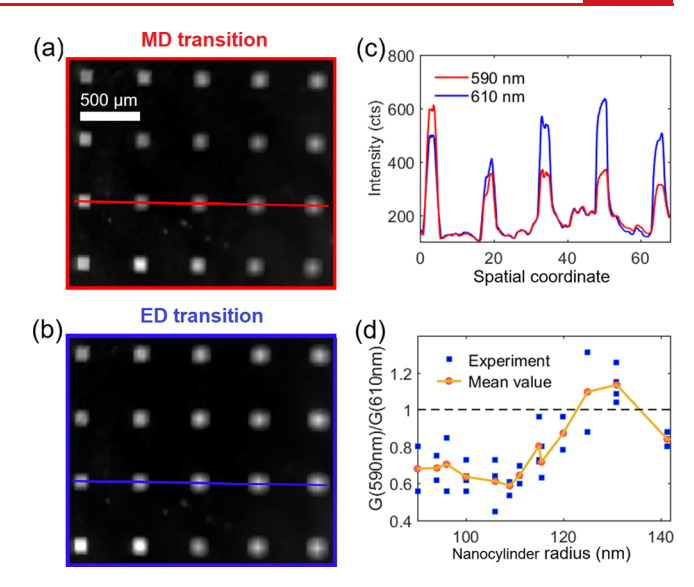


Figure 4. Fluorescence microscopy image of 20 metasurfaces (bright squares, each with a footprint of $100~\mu m \times 100~\mu m$) with different nanocylinder radii covered by a layer of Eu³+ containing polymer observed through narrow bandpass filters with a center wavelength of (a) 590 nm and (b) 610 nm. The images were taken at the same gain settings but different integration times of 4000 ms for the wavelength of 590 nm and 400 ms for the wavelength of 610 nm. (c) Emission intensity along the red and blue horizontal lines shown in (a,b). (d) Experimentally measured emission enhancement ratio G_{590}/G_{610} as a function of the nanocylinder radius.

that is, the bare glass substrate covered by the Eu³⁺ containing polymer layer. Therefore, we can directly compare the enhancement values despite the different intrinsic emission strengths of the electric- and magnetic-dominated transition channels (see Figure 3b).

Both images show the same set of 4×5 metasurfaces having different nanocylinder sizes. The metasurface regions appear brighter than the surrounding glass substrate regions at both wavelengths. We checked that no fluorescence signal was observed from the uncoated metasurfaces under these measurement conditions, so that the enhanced signal can be attributed to the Eu³⁺ emission. Importantly, the absolute enhancement is clearly different for different metasurfaces and different transitions. In order to quantify the differences in fluorescence enhancement in an exemplary fashion, Figure 4c illustrates the fluorescence signals along a horizontal cross section indicated by the red line in Figure 4a and the blue line in Figure 4b. Each of the five peaks shown in Figure 4 corresponds to a particular metasurface. Clearly, metasurfaces with different nanocylinder sizes enhance the magnetic and electric dipole transitions with different efficiency. Most strikingly, the leftmost metasurface in the selected row shows a stronger enhancement for the magnetic-dominated dipole transition, while for all other metasurfaces in the same row, the electric dipole transition is enhanced more strongly.

Next, we perform a systematic analysis of the experimentally measured enhancement values depending on the size of the silicon nanocylinders. The enhancement G_{590} (G_{610}) at the magnetic-dominated (electric) transition wavelength is defined as the ratio of the fluorescence intensity I_{590} (I_{610}) observed for the Eu³⁺ containing polymer layer covering a particular metasurface and the corresponding intensity observed for the same layer on the bare glass substrate next to the metasurface. Figure 4d shows the emission enhancement ratio G_{590}/G_{610} as

a function of the nanocylinder radius. Note that this quantity is closely related to the branching ratios of emission via the magnetic (electric) channel, defined as $\beta_{\rm m} = \frac{I_{\rm 590}}{I_{\rm total}}$ ($\beta_{\rm e} = \frac{I_{\rm 610}}{I_{\rm total}}$), where I_{total} is the total collected fluorescence intensity. While the branching ratio is more commonly used to analyze changes in the transition strength through different decay channels originating from the same upper level, it does not allow for taking reference data from sample areas without any photonic nanostructure into account. Therefore, we base our analysis on the emission enhancement ratio in the following. The solid blue squares correspond to the experimentally measured values of the emission enhancement ratio for individual metasurface arrays, the solid orange circles represent the mean value for several samples with the same nanocylinder radius. Note that we excluded measurement data from two of 40 individual samples, since they were overexposed according to the SEM images. Also note that the enhancement values for different metasurfaces having nominally identical nanocylinder radii are not exactly equal, which is likely due to sample imperfections (e.g., differences in roughness, slight local variations in polymer film thickness or emitter density). However, on average the observed variations in enhancement remain well below the overall changes of the emission enhancement ratio as a function of nanocylinder radius.

Clearly, the mean value of the emission enhancement ratio G_{590}/G_{610} shows a systematic dependence on the nanocylinder radius. The emission enhancement ratio is lower than 1 for the samples with nanocylinder radii below 120 nm, reaching a minimum of 0.6 for the sample with a nanocylinder radius of 109 nm. For larger radii, it then increases and reaches maximum of 1.12 for the sample with a radius of 131 nm. Finally, the emission enhancement ratio decreases again for the sample with even larger nanocylinder radius of 141 nm. This systematic dependence indicates that the enhancement stems from an emission enhancement due to coupling to the Mietype resonances of the metasurfaces as they are shifted in and out of spectral overlap with the electric and magneticdominated transitions of the Eu³⁺ via variation of the radius. Note, however, that there are two different reasons why the emission enhancement ratio G_{590}/G_{610} can deviate from the level of 1, which cannot be distinguished by our experiment alone. Specifically, the emission enhancement observed at 590 and 610 nm can differ due to the different nature of the emission from Eu³⁺ (electric or magnetic dipole) at the two wavelengths, but it could also be influenced by the difference in the emission wavelengths themselves, leading to a change in the spectral overlap with a particular Mie-resonance.

Thus, in order to clarify how the nature of the emission affects the enhancement, we perform numerical simulations to estimate the emission from the metasurfaces covered by a layer of low index polymer incorporating homogeneously distributed point dipole emitters with random orientation. Our method is based on the reciprocity principle. The reciprocity principle can be formulated for a system consisting of two electric point dipoles: $\mathbf{p}_1 \cdot \mathbf{E}_2(\mathbf{r}_1) = \mathbf{p}_2 \cdot \mathbf{E}_1(\mathbf{r}_2)$, where \mathbf{p}_1 is the electric dipole moment of the first dipole placed at position \mathbf{r}_1 and producing an electric field $\mathbf{E}_1(\mathbf{r})$, and \mathbf{p}_2 is the electric dipole moment of the second dipole placed at position \mathbf{r}_2 and producing an electric field $\mathbf{E}_2(\mathbf{r})$. It is also possible to formulate the reciprocity principle for a system consisting of one magnetic and one electric point dipole: $\mathbf{m}_1 \cdot \mathbf{H}_2(\mathbf{r}_1) = \mathbf{p}_2 \cdot \mathbf{E}_1(\mathbf{r}_2)$, where \mathbf{m}_1 is the magnetic dipole moment of the first

dipole placed at position r_1 and producing an electric field $E_1(\mathbf{r})$ and \mathbf{p}_2 is the electric dipole moment of the second dipole placed at position \mathbf{r}_2 and producing a magnetic field $\mathbf{H}_2(\mathbf{r})$. If we place the first dipole \mathbf{p}_1 (\mathbf{m}_1) on our sample and move the second dipole \mathbf{p}_2 far away along the direction (θ, ϕ) , then the $E_1(\mathbf{r}_2)$ represents the far field emitted by the first dipole coupled to the nanocylinder array in the direction (θ, ϕ) and $E_2(\mathbf{r}_1)$ ($H_2(\mathbf{r}_1)$) is the local electric (magnetic) field of the metasurface excited by a plane wave incident from the second dipole along the same direction (θ, ϕ) . Thereby the reciprocity principle allows us to overcome the usual difficulties associated with the simulation of single dipole sources coupled to a periodic structure³⁸ and we are able to limit the computational domain to an elementary cell with periodic boundary conditions. To compare our approach with a more established, yet computationally more demanding, method to calculate the emission properties of a periodic photonic nanostructure, we also performed calculations based on the inverse Floquet transformation.³⁸ The results are included as Supporting Information.

Figure 5a shows a sketch of the elementary cell used in our calculations. The silicon cylinder (blue) is placed onto a glass

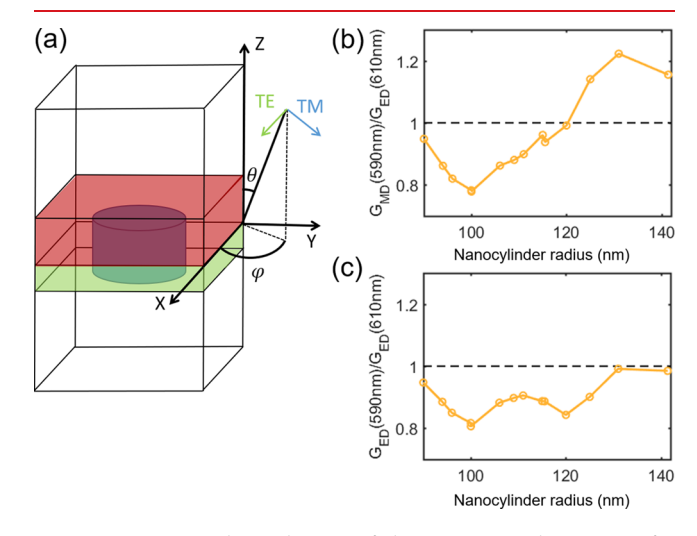


Figure 5. Numerical simulations of the emission enhancement for electric and magnetic dipoles: (a) Sketch of the computational domain. The red and green layers indicate the emitting and the inactive Eu³⁺-containing polymer layers in our simulations. (b) Calculated ratio of the magnetic dipole emission enhancement at 590 nm wavelength and the electric dipole emission enhancement at 610 nm wavelength as a function of nanocylinder radius. (c) Calculated ratio of the electric dipole emission enhancement at 590 nm wavelength and the electric dipole emission enhancement at 610 nm wavelength.

substrate and covered by the Eu^{3+} containing polymer layer (green and red). The polymer was modeled with a refractive index of n=1.6. Note that in the experiment, the excitation field from the 325 nm laser decays inside the active layer, such that the emitters in the upper part of the layer are more efficiently excited. To take this into account in our simulations, we divide the polymer layer into an active upper part (red) of thickness 180 nm and a passive lower part (green) of thickness 40 nm. On the basis of the experimentally measured transmittance of the 325 nm laser light through the polymer layer doped by Eu^{3+} ions, the thickness of the active layer of 180 nm is associated with a decay of the excitation illumination

by a factor of 3. The elementary cell was excited by a plane wave incident from the upper half-space at polar angle θ and azimuthal angle ϕ . The emission enhancement via the magnetic transition $G_{\rm MD}$ can be estimated as 39

$$G_{\text{MD}}(590 \text{ nm}) = \frac{1}{P_{0,\text{MD}}} \sum_{\theta,\phi,\text{TE,TM}} \langle |\mathbf{H}(\mathbf{r}; \theta, \phi)|^2 \rangle \sin \theta$$
(1)

Here, $G_{\rm MD}(590 \, {\rm nm})$ is the emission enhancement from the magnetic dipoles emitting at λ = 590 nm, which are assumed to be randomly oriented and homogeneously distributed inside the active upper part of the polymer layer (red region in Figure 5 (a)). $H(r;\theta,\phi)$ is the local magnetic field excited by either TE or TM polarized plane wave with a wavelength of 590 nm, incident from the upper half-space at polar angle θ and azimuthal angle ϕ . To better match the experimental conditions, only emission under solid angles corresponding to the 0.4NA objective are considered in the summation. \land \cdots \rangle denotes the spatial averaging over the active part of the polymer layer. Similar to the experiment, the calculated emission enhanced by the nanocylinder array is divided by the magnetic dipole emission $P_{0,\mathrm{MD}}$ collected by a 0.4NA objective for the case of a bare glass substrate covered by a Eu3+ containing polymer layer of a thickness of 180 nm (measured by electron microscopy of a focused-ion-beam cross section through the unstructured area of the sample) and calculated using the same approach. Further details on the numerical calculations are included in the Methods. Note that our approach to calculate the numerical emission enhancement ratio as a function of the nanocylinder diameter takes both expected changes of the radiative decay rate and of the collection efficiency into account and is thus directly related to the corresponding fluorescence enhancement observed in experiment. However, it neglects the complex electronic level structure of the Eu3+, the finite quantum efficiencies of the transitions, the details of the excitation regime present in experiment and a possible excitation enhancement. Therefore, it does not allow for a quantitative prediction of the absolute fluorescence enhancement.

Equivalently, for the case of electric dipole emission, we obtain

$$G_{\rm ED}(610~{\rm nm}) = \frac{1}{P_{\rm 0,ED}} \sum_{\theta,\phi,{\rm TE,TM}} \langle |\mathbf{E}(\mathbf{r};\,\theta,\,\phi)|^2 \rangle \sin\theta \tag{2}$$

Here, $G_{\rm ED}(610~{\rm nm})$ is the emission enhancement from the electric dipoles emitting at $\lambda=610~{\rm nm}$, which are also assumed to be randomly oriented and homogeneously distributed inside the active part of the polymer layer. ${\bf E}({\bf r};\theta,\phi)$ is the local electric field excited by either TE or TM polarized plane wave with wavelength of 610 nm, incident from the upper half-space at polar angle θ and azimuthal angle ϕ . $P_{0,{\rm ED}}$ is the electric dipole emission for the case of a bare glass substrate covered by a polymer layer of thickness 180 nm. The collection NA and referencing procedure are the same as for the calculation performed in the case of the magnetic dipole.

We sum over both TE and TM polarizations and the directions of the incident plane wave, while the polar angle of incidence θ takes values in the range of $[0^{\circ},24^{\circ}]$, corresponding to the 0.4NA of the collection objective. The azimuthal angle ϕ that takes values within the range of $[0^{\circ},45^{\circ}]$ corresponding to the symmetry of the two-dimensional square lattice.

Figure 5b shows the calculated emission enhancement ratio $G_{MD}(590 \text{ nm})/G_{ED}(610 \text{ nm})$ as a function of the nanocylinder radius. In our calculations, we used the geometrical parameters of the nanocylinders that provided the best fit for the transmittance spectra of the corresponding sample (see Figure 2). As one can note, we obtain a good qualitative agreement with the experimental data (compare Figure 4d and Figure 5b). Indeed, all the major trends observed in the experimental emission enhancement ratio dependence on the nanocylinder diameter are well reproduced, with only moderate discrepancies in the values.

Note, however, that the absolute values for the emission enhancement appear approximately four times higher in the experiment, independent of the nanocylinder radius (see Supporting Information). This may be due to several reasons. First, the calculations do not consider the level structure of the Eu³⁺, while the fact that the transitions at wavelengths of 590 and 610 nm, as well as several other transition lines originate from the same upper level leads to additional competitive enhancement and depletion mechanisms.³ Second, a possible excitation enhancement by the nanocylinder arrays can increase the fluorescence signal in experiments. The proper implementation of excitation enhancement in calculations is not possible due to the lack of the dispersion data in UV for the material of the nanocylinders and due to the complex illumination configuration. Third, sample imperfections affect the near fields and cause additional scattering, which can potentially enhance the outcoupling and collection efficiency in the experiment. In particular, the upper surface of the Eu³⁺ containing layer is assumed as flat in the numerical model, while it shows a wavy structure in experiment (see Figure 3c). Finally, the orientation or distribution of the Eu³⁺ ions within the polymer layer may be inhomogeneous. Importantly, the two factors which we deem most severe, namely the possible excitation enhancement and the underestimation of the outcoupling efficiency, affect the data independent of the type of the transition (electric or magnetic). Therefore, in contrast to the absolute enhancement values the emission enhancement ratio is not impacted by these factors. Thus, we have chosen it as our primary experimental observable.

As a final step, we also calculated the emission enhancement ratio $G_{\rm ED}(590 \, {\rm nm})/G_{\rm ED}(610 \, {\rm nm})$ at a wavelength of 590 nm assuming that the emission originates purely from electric dipole transition by replacing the magnetic field in eq 1 by the electric field. This result is shown in Figure 5c. One can note that the behavior of the experimental data in Figure 4d is qualitatively different compared to the calculations assuming electric dipole emission at 590 nm wavelength. This result underpins that the fluorescence maximum at 590 nm in the Eu³⁺ spectrum remains magnetic-dipole dominated also in the presence of the metasurface. On the basis of our numerical simulations, we can conclude that the change of the emission enhancement ratio as a function of thenanocylinder diameter will be mainly due to the different dipolar nature of the two transitions, while the mere difference in emission wavelength plays a minor role.

In conclusion, we have experimentally demonstrated the enhancement of the spontaneous emission of Eu³⁺ ions by dielectric metasurfaces composed of Mie-resonant silicon nanocylinders. By fabricating metasurfaces featuring different nanocylinder radii, we have swept the position of Mie resonances having a strong quadrupolar contribution over the spectral range of the electric and magnetic-dominated

dipole transitions of the Eu³⁺. We have observed a systematic change of the branching ratio of emission via the two different channels. Especially, we have experimentally shown, for the first time, that Mie-resonant all-dielectric metasurfaces allow for selective enhancement of the magnetic dipole emission over the electric dipole emission for a proper choice of the metasurface geometry. We have confirmed our observations with numerical simulations. Our results on the manipulation of magnetic dipole emission by designed resonant photonic nanostructures open new pathways for future research on magnetic light-matter interactions in the fields of active dielectric nanophotonics, light-emitting metasurfaces, and nanoantennas, as well as for novel photonic materials and devices exploiting magnetic dipole transitions. 40,41 More generally, enhancing interactions with the magnetic component of light is of fundamental scientific interest because it adds a new degree of freedom in photonics and optoelectronics, thus allowing to independently test phenomena, which are already well studied for the electric component of light, in the dual-symmetric setting. Moreover, the magnetic component of light is essential in chiral light-matter interactions, including chiral sensing 42 and chiral emission phenomena. 43,44

While the a-Si:H material used for fabrication of the metasurfaces exhibits non-negligible absorption losses at both emission wavelengths, even larger total enhancements and higher radiation efficiencies will become possible through the development of new high-index dielectric material platforms such as gallium phosphide. 45

Methods. Sample Fabrication. For fabrication of silicon disks on the glass substrate we first deposit thin-films of hydrogenated amorphous silicon (a-Si:H) with a thickness of 182 nm, using plasma-enhanced chemical vapor deposition (PECVD) at a temperature of 250 °C on standard microscope coverslips. Next, the substrates are spin-coated with the negative-tone electron-beam resist maN-2403. The nanocylinders are then defined by electron-beam lithography (EBL) in combination with inductively coupled plasma (ICP) etching of the silicon thin-film, where the exposed electron-beam resist is used as an etch mask. As etch gases, we used SF₆ (1.8 sccm) and CHF₃ (50 sccm). Etching was performed at 20 °C with 10 mTorr at 500 W induction power and 15 W bias power. Finally, residual resist and organic solvent residue left on the sample were removed using oxygen plasma. To render the sample conductive for imaging with an electron microscope, we cover it with a thin (15 nm) transparent layer of indium tin oxide (ITO) using sputter coating at 1.5 mTorr pressure, 20 sccm argon flow, 60 W power, and 8×10^{-7} Torr base pressure.

Transmittance Simulations. An elementary unit cell with Floquet periodic boundary conditions and two ports, one at the top and one at the bottom, was used. The top port acted as a source exciting a normally incident plane wave. The reflected, transmitted and diffracted light was detected by both ports. The glass substrate was modeled with a refractive index of n = 1.51. For the optical material parameters of the a-Si:H, we used experimental data obtained from ellipsometry measurements on unstructured a-Si:H films.

■ ASSOCIATED CONTENT

S Supporting Information

The Supporting Information is available free of charge on the ACS Publications website at DOI: 10.1021/acs.nanolett.8b04268.

Table of the metasurface geometrical parameters used in numerical calculations. Description of the experimental setup. Multipole analysis of the modes excited in nanocylinders. Inverse Floquet transformation for far-field emission calculations. Experimental and numerical results for the electric and magnetic emission enhancement (absolute values). (PDF)

AUTHOR INFORMATION

Corresponding Author

*E-mail: aleksandr.vaskin@uni-jena.de.

ORCID 🏻

Aleksandr Vaskin: 0000-0002-3014-1002

 $Ivan\ Fernandez\text{-}Corbaton:\ 0000\text{-}0003\text{-}2834\text{-}5572$

Yuri S. Kivshar: 0000-0002-3410-812X Dragomir N. Neshev: 0000-0002-4508-8646 Isabelle Staude: 0000-0001-8021-572X

Notes

The authors declare no competing financial interest.

ACKNOWLEDGMENTS

Financial support by the Thuringian State Government within its ProExcellence initiative (ACP²⁰²⁰) and the German Research Foundation (STA 1426/2-1) is gratefully acknowledged. K.E.C., D.N.N., and Y.S.K. acknowledge the support by the Australian Research Council (DP150103733). Y.S.K. acknowledges a support from the Alexander von Humboldt Foundation. S.N. acknowledges financial support by the Karlsruhe School of Optics and Photonics and by the DFG Priority Programm 1839 Tailored Disorder. The authors also acknowledge their participation in the Erasmus Mundus NANOPHI project, contract number 2013 5659/002-001. N.N., M.A.N., and S.M. would like to acknowledge the support by NSF EiR grant # 1830886. This work was performed in part at the ACT node of the Australian National Fabrication Facility, a company established under the National Collaborative Research Infrastructure Strategy to provide nano- and microfabrication facilities for Australia's researchers. We are grateful to the company JCMwave for their free provision of the FEM Maxwell solver JCMsuite with which the Floquet simulations in this work have been performed. We acknowledge fruitful discussions with M. Decker.

■ REFERENCES

- (1) Giessen, H.; Vogelgesang, R. Glimpsing the Weak Magnetic Field of Light. *Science* **2009**, 326, 529–530.
- (2) Burresi, M.; van Oosten, D.; Kampfrath, T.; Schoenmaker, H.; Heideman, R.; Leinse, A.; Kuipers, L. *Science* **2009**, 326, 550–553.
- (3) Taminiau, T. H.; Karaveli, S.; van Hulst, N. F.; Zia, R. Quantifying the magnetic nature of light emission. *Nat. Commun.* **2012**, *3*, 979.
- (4) Kasperczyk, M.; Person, S.; Ananias, D.; Carlos, L. D.; Novotny, L. Excitation of magnetic dipole transiitons at optical frequencies. *Phys. Rev. Lett.* **2015**, *114*, 163903.
- (5) Brewer, N. R.; Buckholtz, Z. N.; Simmons, Z. J.; Mueller, E. A.; Yavuz, D. D. Coherent magnetic response at optical frequencies using atomic transitions. *Phys. Rev. X* **2017**, *7*, 011005.
- (6) Purcell, E. M. Spontaneous emission probabilities at radio frequencies. *Phys. Rev.* **1946**, *69*, 681.
- (7) Baranov, D. G.; Savelev, R. S.; Li, S. V.; Krasnok, A. E.; Alú, A. Modifying magnetic dipole spontaneous emission with nanophotonic structures. *Laser Photonics Rev.* **2017**, *11*, 1600268.

(8) Noginova, N.; Zhu, G.; Mayy, M.; Noginov, M. A. Magnetic dipole based systems for probing optical magnetism. *J. Appl. Phys.* **2008**, *103*, 07E901.

- (9) Karaveli, S.; Zia, R. Spectral Tuning by Selective Enhancement of Electric and Magnetic Dipole Emission. *Phys. Rev. Lett.* **2011**, *106*, 193004.
- (10) Ni, X.; Naik, G. V.; Kildishev, A. V.; Barnakov, Y.; Boltasseva, A.; Shalaev, V. M. Effect of metallic and hyperbolic metamaterial surfaces on electric and magnetic dipole emission transitions. *Appl. Phys. B: Lasers Opt.* **2011**, *103*, 553.
- (11) Hussain, R.; Keene, D.; Noginova, N.; Durach, M. Spontaneous emission of electric and magnetic dipoles in the vicinity of thin and thick metal. *Opt. Express* **2014**, *22*, 7744.
- (12) Aigouy, L.; Cazé, A.; Gredin, P.; Mortier, M.; Carminati, R. Mapping and Quantifying Electric and Magnetic Dipole Luminescence at the Nanoscale. *Phys. Rev. Lett.* **2014**, *113*, 076101.
- (13) Hussain, R.; Kruk, S. S.; Bonner, C. E.; Noginov, M. A.; Staude, I.; Kivshar, Y. S.; Noginova, N.; Neshev, D. N. Enhancing Eu³⁺ magnetic dipole emission by resonant plasmonic nanostructures. *Opt. Lett.* **2015**, *40*, 1659.
- (14) Choi, B.; Iwanaga, M.; Sugimoto, Y.; Sakoda, K.; Miyazaki, H. T. Selective Plasmonic Enhancement of Electric- and Magnetic-Dipole Radiations of Er Ions. *Nano Lett.* **2016**, *16*, 5191–5196.
- (15) Murai, S.; Saito, M.; Sakamoto, H.; Yamamoto, M.; Kamakura, R.; Nakanishi, T.; Fujita, K.; Verschuuren, M. A.; Hasegawa, Y.; Tanaka, K. Directional outcoupling of photoluminescence from Eu(III)-complex thin films by plasmonic array. *APL Photon* **2017**, *2*, 026104.
- (16) Kuznetsov, A. I.; Miroshnichenko, A. E.; Brongersma, M. L.; Kivshar, Y. S.; Lukyanchuk, B. Optically resonant dielectric nanostructures. *Science* **2016**, *354*, aag2472.
- (17) Decker, M.; Staude, I. Resonant dielectric nanostructures: A low-loss platform for functional nanophotonics. *J. Opt.* **2016**, *18*, 103001
- (18) Jahani, J.; Jacob, Z. All-dielectric metamaterials. Nat. Nanotechnol. 2016, 11, 23.
- (19) Staude, I.; Schilling, J. Metamaterial-inspired silicon nano-photonics. *Nat. Photonics* **2017**, *11*, 274.
- (20) Kruk, S.; Kivshar, Y. S. Functional meta-optics and nanophotonics governed by Mie resonances. *ACS Photonics* **2017**, *4* (11), 2638–2649.
- (21) Neshev, D. N.; Aharonovich, I. Optical metasurfaces: new generation building blocks for multi-functional optics. *Light: Sci. Appl.* **2018**, *7*, 2047.
- (22) Rolly, B.; Bebey, B.; Bidault, S.; Stout, B.; Bonod, N. Promoting magnetic dipolar transition in trivalent lanthanide ions with lossless Mie resonances. *Phys. Rev. B: Condens. Matter Mater. Phys.* **2012**, *85*, 245432.
- (23) Schmidt, M. K.; Esteban, R.; Sáenz, J. J.; Suárez-Lacalle, I.; Mackowski, S.; Aizpurua, J. Dielectric antennas a suitable platform for controlling magnetic dipolar emission. *Opt. Express* **2012**, *20*, 13636.
- (24) Zambrana-Puyalto, X.; Bonod, N. Purcell factor of spherical Mie resonators. *Phys. Rev. B: Condens. Matter Mater. Phys.* **2015**, 91, 195422
- (25) Feng, T.; Xu, Y.; Liang, Z.; Zhang, W. All-dielectric hollow nanodisk for tailoring magnetic dipole emission. *Opt. Lett.* **2016**, *41*, 5011.
- (26) Li, J.; Verellen, N.; Van Dorpe, P. Enhancing Magnetic Dipole Emission by a Nano-Doughnut-Shaped Silicon Disk. *ACS Photonics* **2017**, *4* (8), 1893–1898.
- (27) Sanz-Paz, M.; Ernandes, C.; Esparza, J. U.; Burr, G. W.; van Hulst, N. F.; Maitre, A.; Aigouy, L.; Gacoin, T.; Bonod, N.; Garcia-Parajo, M. F.; Bidault, S.; Mivelle, M. Enhancing Magnetic Light Emission with All-Dielectric Optical Nanoantennas. *Nano Lett.* **2018**, *18* (6), 3481–3487.
- (28) Wiecha, P. R.; Majorel, C.; Girard, C.; Arbouet, A.; Masenelli, B.; Boisron, O.; Lecestre, A.; Larrieu, G.; Paillard, V.; Cuche, A. Enhancement of electric and magnetic dipole transition of rare-earth

doped thin films tailored by high-index dielectric nanostructures. *Phys. Rev. B: Condens. Matter Mater. Phys.* **2018**, 97, 09690.

- (29) Vaskin, A.; Bohn, J.; Chong, K. E.; Bucher, T.; Zilk, M.; Choi, D.-Y.; Neshev, D. N.; Kivshar, Y. S.; Pertsch, T.; Staude, I. Directional and Spectral Shaping of Light Emission with Mie-Resonant Silicon Nanoantenna Arrays. ACS Photonics 2018, 5 (4), 1359–1364.
- (30) Bohn, J.; Bucher, T.; Chong, K. E.; Komar, A.; Choi, D.-Y.; Neshev, D. N.; Kivshar, Y. S.; Pertsch, T.; Staude, I. Active Tuning of Spontaneous Emission by Mie-Resonant Dielectric Metasurfaces. *Nano Lett.* **2018**, *18* (6), 3461–3465.
- (31) Liu, S.; Vaskin, A.; Addamane, S.; Leung, B.; Tsai, M.-C.; Yang, Y.; Vabishchevich, P. P.; Keeler, G. A.; Wang, G.; He, X.; Kim, Y.; Hartmann, N. F.; Htoon, H.; Doorn, S. K.; Zilk, M.; Pertsch, T.; Balakrishnan, G.; Sinclair, M. B.; Staude, I.; Brener, I. Light-Emitting Metasurfaces: Simultaneous Control of Spontaneous Emission and Far-Field Radiation. *Nano Lett.* **2018**, *18* (11), 6906–6914.
- (32) Grahn, P.; Shevchenko, A.; Kaivola, M. Electromagnetic multipole theory for optical nanomaterials. *New J. Phys.* **2012**, *14*, 093033.
- (33) Arslan, D.; Chong, K. E.; Miroshnichenko, A. E.; Choi, D.-Y.; Neshev, D. N.; Pertsch, T.; Kivshar, Y. S.; Staude, I. Angle-selective all-dielectric Huygens' metasurfaces. *J. Phys. D: Appl. Phys.* **2017**, *50*, 434002.
- (34) Wang, K.; Gao, L.; Huang, C. Optical properties of the highly ordered Langmuir-Blodgett film of a strongly luminescent Eu(III) complex. *J. Photochem. Photobiol., A* **2003**, *156* (1–3), 39–43.
- (35) Tsaryuk, V. I.; Zhuravlev, K. P.; Zolin, V. F.; Kudryashova, V. A.; Legendziewicz, J.; Szostak, R. Luminescence efficiency of aromatic carboxylates of europium and terbium. *J. Appl. Spectrosc.* **2007**, *74*, 51.
- (36) Landau, L. D.; Lifshits, E. M.; Pitaevskii, L. Electrodynamics of continuous media; Pergamon Press: Oxford, 1984; Vol. 8.
- (37) Kahl, M.; Voges, E. Analysis of plasmon resonance and surface-enhanced Raman scattering on periodic silver structures. *Phys. Rev. B: Condens. Matter Mater. Phys.* **2000**, *61*, 14078.
- (38) Burger, S.; Zschiedrich, L.; Greiner, H. J.; Schmidt, F. Numerical analysis of nanostructures for enhanced light extraction from OLEDs. *Proc. SPIE* **2013**, 8641.
- (39) Zhang, S.; Martins, E. R.; Diyaf, A. G.; Wilson, J. I. B.; Turnbull, G. A.; Samuel, I. D. W. Calculation of the emission power distribution of microstructured OLEDs using the reciprocity theorem. *Synth. Met.* **2015**, 205, 127.
- (40) Zia, R. Enhanced Magnetic Ddipole Transitions in Lanthanide Materials for Optics and Photonics. US Patent App. 2011, 12/998,599.
- (41) Zia, R.; Cueff, S.; Karaveli, S. High frequency light emission device. US Patent App. 2017, 14/668,327.
- (42) Ho, C.-S.; Garcia-Etxarri, A.; Zhao, Y.; Dionne, J. Enhancing Enantioselective Absorption Using Dielectric Nanospheres. *ACS Photonics* **2017**, *4*, 197–203.
- (43) Klimov, V. V.; Guzatov, D. V.; Ducloy, M. Engineering of radiation of optically active molecules with chiral nano-meta-particles. *EPL* **2012**, *97*, 47004.
- (44) Gong, S.-H.; Alpeggiani, F.; Sciacca, B.; Garnett, E. C.; Kuipers, L. Nanoscale chiral valley-photon interface through optical spin-orbit coupling. *Science* **2018**, 359 (6374), 443–447.
- (45) Cambiasso, J.; Grinblat, G.; Li, Y.; Rakovich, A.; Cortés, E.; Maier, S. A. Bridging the Gap between Dielectric Nanophotonics and the Visible Regime with Effectively Lossless Gallium Phosphide Antennas. *Nano Lett.* **2017**, *17* (2), 1219–1225.